Stability Analysis of PLL Influenced by Control Loops in Grid-connected Converters Under Fault Disturbance

Yushuang Liu, Meng Huang, Xiaoming Zha, and Herbert Ho-Ching Iu, *Senior Member, IEEE*

***Abstract*—When the power grid suffers from grid faults that cause phase disturbances, the grid-connected converter becomes destabilized by the interaction between the phase-locked loop (PLL) and the control loop. In this paper, the stability of the PLL affected by the control loop under transient grid faults is studied. First, the equivalent model of the PLL under the influence of the control loop is established. Then, different response processes of PLLs under the ground fault with various control parameters are qualitatively analyzed. Furthermore, a small-signal model is proposed to assess the stability of the PLL under different control loop parameters. The system poles can be calculated to show the physical origin of the instability. Finally, simulations of a three-phase 21-level modular multilevel converter (MMC) built in PSCAD and a down-scale experiment is performed to verify the parameter influence of the control loop on the PLL.**

***Index Terms*—Control loop, grid-connected MMC, ground fault, phase-locked loop, transient stability.**

I. Introduction

With the increasing application of power electronic devices in the power system, operational characteristics of power systems have changed tremendously due to the introduction of such devices [1]–[4]. For example, when a fault occurs in the power grid, the fault may have an adverse influence on the operation of grid-connected converters, and then the dynamic behaviors of converters may further exacerbate the operation of the whole power system. To ensure the safe operation of power systems, stability issues of power electronic-based power systems have received increasing attention during recent years [5]–[8].

Considering that grid faults always bring severe problems to power electronic-based power systems, such as overcurrent, overvoltage and some oscillation behaviors [9]–[11], studying how grid faults impact converters that are connected to weak AC grids becomes a popular research area [12]–[14]. From most of this research, the behaviors of phase-locked loops (PLLs) have been revealed to analyze the impact on the stability of converters [15], [16], since the PLL is adopted to detect the voltage phase at the point of common coupling (PCC) to synchronize converters to the power grid [17].

A great amount of research has been done investigating the small-signal stability analysis of PLLs to predict their low-frequency unstable oscillations in grid-connected converter systems [18]. During the process of small-signal analysis, small-signal linearization methods and linear control theories are utilized to simplify the analysis [19]. For example, a unified small-signal impedance model of grid-connected voltage-source converters (VSCs) is established in [20], to predict the stability impact of the PLL. In [21], the linearized grid-synchronization loop and the self-synchronization loop are proposed to explain the interaction of the power grid and the injection current in a grid-connected VSC. However, the small-signal analysis can only predict the stability of PLLs around steady-states and cannot reflect the failure process and instability mechanism under grid faults.

To study the instability process of the PLL under faults, transient stability analysis is needed. Some literature uses power-angle curves or voltage-angle curves to describe the transient process of PLLs in different scenarios [19], [22]–[24]. In a grid-connected converter system without current limitation, phase-portrait analysis is adopted to study the transient responses of the converter with a power synchronization control [22], [23]. In a current limited grid-connected converter system, the converter reaching the current limitation can be regarded as a current source which is only controlled by the reference current. The dynamic behavior of PLLs in such situations has been analyzed in [19]. However, in this research, the control loops are simplified or ignored. In [25], a current loop with a voltage feedforward filter is adopted to prevent instability of the grid-connected system, but the dynamic responses of the PLL are ignored. In a previous work that considers both the control loop and the PLL [16], the response of the PLL influenced by the control loop is neglected. In practical grid-connected systems, the behaviors of PLLs may be influenced by the widely-used inner current loop and outer power/voltage loop. Hence, analyzing the transient stability of the PLL considering the influence of the dynamics of the control loop under grid faults is of great significance.

In this paper, the PLL affected by the current loop and the power loop in a grid-connected modular multilevel converter (MMC) is taken into consideration. The outline of this paper is

Manuscript received October 25, 2019; revised December 24, 2019; accepted January 3, 2020. Date of online publication February 13, 2020; date of current version March 18, 2020. This work was supported by the National Natural Science Foundation of China (51877159, 51637007, U1866601).

Y. Liu, M. Huang (corresponding author, e-mail: meng.huang@whu.edu.cn), and X. Zha are with the School of Electrical Engineering and Automation, Wuhan University, Wuhan 430000, China.

H. H.-C. Iu is with the School of Electrical, Electronic and Computer Engineering, The University of Western Australia, Crawley WA 6009, Australia.

DOI: 10.17775/CSEEJPES.2019.02760

arranged as follows. In Section II, the equivalent model of the PLL is established to present the interaction with the control loop. In Section III, the transient process of how the control loop influences the PLL under the ground fault is clarified. In Section IV, a small-signal analysis model is proposed to assess the stability of the PLL after a ground fault under different control loop parameters. In Section V, simulations of a grid-connected three-phase 21-level MMC built in PSCAD are performed to analyze the parameter influence and verify the analysis above. Section VI provides our conclusions.

II. Equivalent Model of PLL

In order to study the stability of the PLL influenced by the control loop under grid faults, a grid-connected MMC system disturbed by a grid ground fault is presented in this paper. The system is shown in Fig. 1. The AC grid is a non-ideal power grid, where $Z_{\rm g}$, $Z_{\rm line1}$ and $Z_{\rm line2}$ are the inner impedances of the AC grid. $Z_{\rm g}$ represents the equivalent impedance of series transmission lines in the power grid, while $Z_{\rm line1}$ and $Z_{\rm line2}$ represent the impedances of two paralleled transmission lines (line 1 and line 2). The MMC is connected to the AC grid at the point of common coupling (PCC), as shown in Fig. 1. $Z_{\rm f}$ is the impedance of the AC filter. $Z_{\rm gnd}$ is the ground impedance. The topology of the three-phase MMC is shown in Fig. 2.

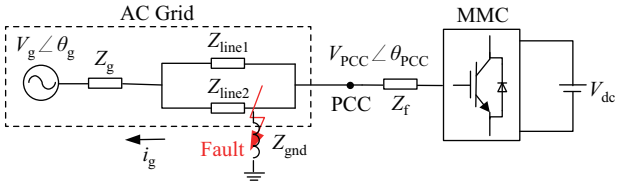

Fig. 1. Grid-connected MMC system.

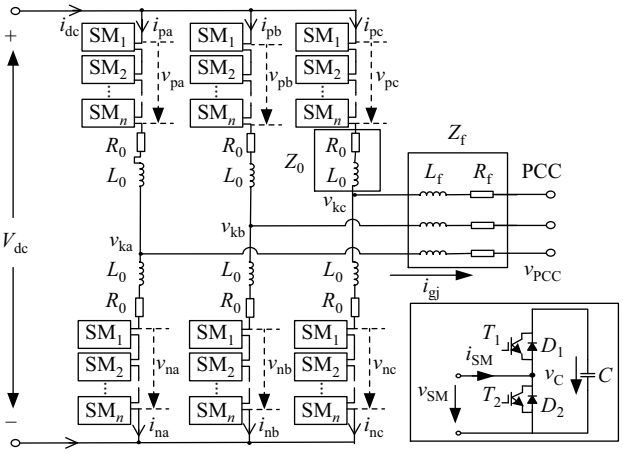

Fig. 2. Topology of three-phase MMC.

To analyze the stability of the PLL in the grid-connected three-phase MMC system under a grid fault, the phasor diagram is shown in Fig. 3. The black arrows represent the voltage vectors before the fault and the red arrows represent the voltage vectors after the fault. In the phasor diagram, it can be seen that the ground fault leads to a phase jump, since the grid impedance $Z_{\rm s}$ changes from $Z_{\rm s1}$ to $Z_{\rm s2}$, where $Z_{\rm s1} = Z_{\rm g} + (Z_{\rm line1}//Z_{\rm line2})$ before the fault and $Z_{\rm s} = Z_{\rm s2} = Z_{\rm s1}//Z_{\rm gnd}$ after the fault.

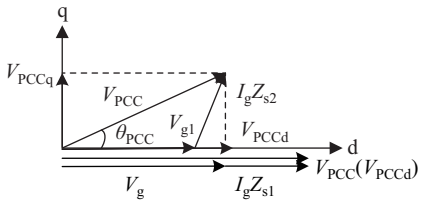

Fig. 3. Phasor diagram before and after fault.

Before the fault, the voltage drop on the grid inductance $L_{\rm s1}$ can be ignored. Due to the effect of the PLL, the phase angle of the voltage at PCC $\theta_{\rm PCC}$, the output phase angle of the PLL $\theta_{\rm PLL}$ and the grid phase $\theta_{\rm g}$ can be regarded as the same, i.e., $\theta_{\rm PCC} = \theta_{\rm PLL} = \theta_{\rm g}$. Thus, the system operates with a unity power factor before the fault, in which case the voltage at PCC can be given as:

$$V_{\rm PCC}\angle\theta_{\rm PCC} = V_{\rm g}\angle\theta_{\rm g} + I_{\rm g}Z_{\rm s1}\angle\theta_{\rm g} \tag{1}$$

However, when the fault happens, the grid impedance $Z_{\rm s}$ will become smaller (i.e. $Z_{\rm s2}$), and the phase angle of the grid impedance $\theta_{\rm s2}$ may change suddenly. The phases $\theta_{\rm PCC}$, $\theta_{\rm PLL}$ and $\theta_{\rm g}$ are unable to stay the same any more.

Figure 4 shows the Norton equivalent circuit of the AC grid after the ground fault. The amplitude ofequivalent grid voltage would drop to $V_{\rm g1} = V_{\rm g}Z_{\rm s2}/Z_{\rm s1}$. Ignoring the phase variation of the equivalent grid voltage $v_{\rm g1}$ and assuming the grid current $i_{\rm g}$ remains unchanged, the amplitude of voltage at PCC $V_{\rm PCC}$ would decrease, as shown in Fig. 3. The PCC voltage in d-axis $v_{\rm PCCd}$ may decline with the drop of $V_{\rm PCC}$, and the PCC voltage in q-axis $v_{\rm PCCq}$ may slightly increase with the growth of the phase angle $\theta_{\rm PCC}$. The PCC voltage at the moment of the fault happening can be calculated as:

$$V_{\rm PCC}\angle\theta_{\rm PCC} = V_{\rm g1}\angle\theta_{\rm g} + I_{\rm g}Z_{\rm s2}\angle(\theta_{\rm g} + \theta_{\rm s2}) \tag{2}$$

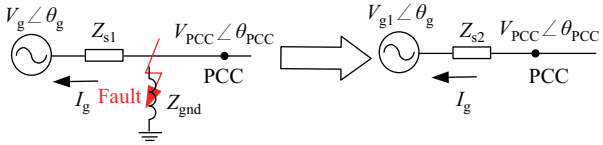

Fig. 4. Norton equivalent circuit of the AC grid after ground fault.

After the fault, the PLL and the control loop work to adjust the operational state of the MMC system which is connected to a weak power grid. We can establish a two-source equivalent circuit of this grid-connected system after the fault as shown in Fig. 5.

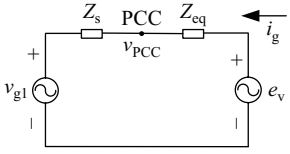

Fig. 5. Two-source equivalent circuit.

Figure 5 shows that the voltage at PCC v_{PCC} is affected by both the equivalent grid voltage v_{g1} and the equivalent output voltage of the MMC e_{v}. Z_{s} and Z_{eq} represent the grid impedance and the equivalent impedance of the MMC respectively, where $Z_{\mathrm{eq}} = Z_{\mathrm{f}} + Z_0/2$. According to the two-source equivalent circuit of the MMC system, the voltage at PCC can be obtained as:

$$V_{\mathrm{PCC}}\angle\theta_{\mathrm{PCC}} = \frac{Z_{\mathrm{eq}}(\omega_{\mathrm{g}})}{Z_{\mathrm{s}}(\omega_{\mathrm{g}}) + Z_{\mathrm{eq}}(\omega_{\mathrm{g}})} V_{\mathrm{g1}}\angle(\theta_{\mathrm{g}} + \varphi_1) + \frac{Z_{\mathrm{s}}(\omega_{\mathrm{PLL}})}{Z_{\mathrm{s}}(\omega_{\mathrm{PLL}}) + Z_{\mathrm{eq}}(\omega_{\mathrm{PLL}})} E_{\mathrm{v}}\angle(\theta_{\mathrm{v}} + \varphi_2) \quad (3)$$

$$\begin{cases} K_1(\omega) = \left| \dfrac{Z_{\mathrm{eq}}(\omega)}{Z_{\mathrm{s}}(\omega) + Z_{\mathrm{eq}}(\omega)} \right| \\ K_2(\omega) = \left| \dfrac{Z_{\mathrm{s}}(\omega)}{Z_{\mathrm{s}}(\omega) + Z_{\mathrm{eq}}(\omega)} \right| \end{cases} \quad (4)$$

$$\begin{cases} \varphi_1 = \mathrm{phase}\left(\dfrac{Z_{\mathrm{eq}}}{Z_{\mathrm{s}} + Z_{\mathrm{eq}}}\right) \\ \quad = \arctan \dfrac{\omega L_{\mathrm{eq}} R_{\mathrm{s}} - \omega L_{\mathrm{s}} R_{\mathrm{eq}}}{R_{\mathrm{eq}}(R_{\mathrm{eq}} + R_{\mathrm{s}}) + \omega^2 L_{\mathrm{eq}}(L_{\mathrm{eq}} + L_{\mathrm{s}})} \\ \varphi_2 = \mathrm{phase}\left(\dfrac{Z_{\mathrm{s}}}{Z_{\mathrm{s}} + Z_{\mathrm{eq}}}\right) \\ \quad = \arctan \dfrac{\omega L_{\mathrm{s}} R_{\mathrm{eq}} - \omega L_{\mathrm{eq}} R_{\mathrm{s}}}{R_{\mathrm{s}}(R_{\mathrm{eq}} + R_{\mathrm{s}}) + \omega^2 L_{\mathrm{s}}(L_{\mathrm{eq}} + L_{\mathrm{s}})} \end{cases} \quad (5)$$

where E_{v} represents the amplitude of the MMC equivalent output voltage e_{v}. ω_{g} is the angular frequency of the power grid and ω_{PLL} is the output angular frequency of the PLL.

Transforming v_{PCC} into *dq* rotating reference frame, the dq-axis voltage of v_{PCC} can be calculated as:

$$\begin{cases} v_{\mathrm{PCCd}} = K_1(\omega_{\mathrm{g}}) V_{\mathrm{g1}} \cos[\theta_{\mathrm{g}} + \varphi_1(\omega_{\mathrm{g}}) - \theta_{\mathrm{PLL}}] \\ \qquad + K_2(\omega_{\mathrm{PLL}}) E_{\mathrm{v}}(\omega_{\mathrm{PLL}}) \cos[\theta_{\mathrm{v}} + \varphi_2(\omega_{\mathrm{g}}) - \theta_{\mathrm{PLL}}] \\ v_{\mathrm{PCCq}} = K_1(\omega_{\mathrm{g}}) V_{\mathrm{g1}} \sin[\theta_{\mathrm{g}} + \varphi_1(\omega_{\mathrm{g}}) - \theta_{\mathrm{PLL}}] \\ \qquad + K_2(\omega_{\mathrm{PLL}}) E_{\mathrm{v}}(\omega_{\mathrm{PLL}}) \sin[\theta_{\mathrm{v}} + \varphi_2(\omega_{\mathrm{g}}) - \theta_{\mathrm{PLL}}] \end{cases} \quad (6)$$

Based on the control block of the PLL presented in Fig. 6, the output phase angle of the PLL is obtained from a PI and an integral process. Thus, the output phase angle can be written as:

$$\theta_{\mathrm{PLL}} = \int [\omega_{\mathrm{g}} + (K_p + K_i \int) v_{\mathrm{PCCq}}] \quad (7)$$

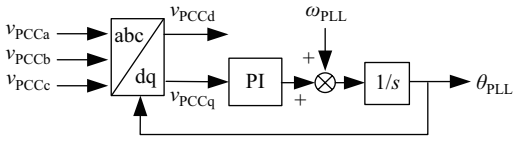

Fig. 6. Control diagram of PLL.

Substituting (6) into (7), the control equation of the PLL can be rewritten as:

$$\theta_{\mathrm{PLL}} = \int \{\omega_{\mathrm{g}} + (K_p + K_i \int)[K_1 V_{\mathrm{g1}} \sin(\theta_{\mathrm{g}} + \varphi_1 - \theta_{\mathrm{PLL}}) + K_2 E_{\mathrm{v}} \sin(\theta_{\mathrm{v}} + \varphi_2 - \theta_{\mathrm{PLL}})]\} \quad (8)$$

Since the phase angle of the equivalent output voltage θ_{v} is provided by the PLL, θ_{v} is regarded as equal to θ_{PLL} in this paper. Considering the voltage drop on the impedance $I_{\mathrm{g}} Z_{\mathrm{s}}$ is far smaller than the equivalent grid voltage v_{g1}, the phase angle of the PCC voltage θ_{PCC} can be regarded as equal to the grid phase θ_{g}, i.e., $\theta_{\mathrm{PCC}} \approx \theta_{\mathrm{g}}$. Define the phase angle difference between θ_{PLL} and θ_{PCC} as δ, there is:

$$\delta = \theta_{\mathrm{PCC}} - \theta_{\mathrm{PLL}} \approx \theta_{\mathrm{g}} - \theta_{\mathrm{PLL}} \quad (9)$$

Thus, the equivalent model of the PLL can be expressed as:

$$\delta = \int \{(K_p + K_i \int)[K_1 V_{\mathrm{g1}} \sin(\varphi_1 + \delta) + K_2 E_{\mathrm{v}} \sin \varphi_2]\} \quad (10)$$

which reflects the PLL behavior under the influence of the grid impedance and the output voltage of the control loop. Based on (10), the control block of the PLL considering the interaction of the control loop after the grid fault can be plotted, as shown in Fig. 7.

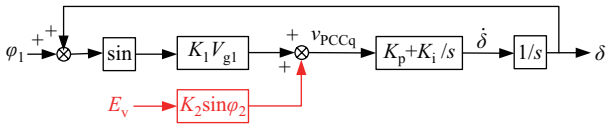

Fig. 7. Control diagram of PLL with the interaction of the control loop.

Assuming that the equivalent output voltage of the MMC is equal to the output command of the control loop, i.e., $e_{\mathrm{v}} \approx e_{\mathrm{v}}^*$, the red part in Fig. 7 represents the effect of the control loop on the PLL. Actually, in many researchers' previous works, the output voltage or current of the converter is always given as a constant, which may not be disturbed by the grid fault and cannot reflect the influence of the control loop. However, in this paper, the variation of E_{v} after the fault, which shows the dynamic of the control loop, is considered.

III. Influence of Control Loop

From the analysis in Section II, it can be shown that the d-axis voltage v_{PCCd} would decrease and the q-axis voltage v_{PCCq} slightly increase when a ground fault happens in line2, which will lead to the increasing of $\dot{\delta}$ and δ. The variation of v_{PCCd} and v_{PCCq} will also cause the action of both the inner current loop and outer power loop.

According to the control diagram of the outer voltage loop in Fig. 8, the control equation is given as:

$$\begin{cases} i_{\mathrm{dref}} = (K_{p2} + K_{i2} \int)\left(P_{\mathrm{ref}} - \dfrac{3}{2} i_{\mathrm{d}} v_{\mathrm{PCCd}} - \dfrac{3}{2} i_{\mathrm{q}} v_{\mathrm{PCCq}}\right) \\ i_{\mathrm{qref}} = (K_{p2} + K_{i2} \int)\left(Q_{\mathrm{ref}} - \dfrac{3}{2} i_{\mathrm{q}} v_{\mathrm{PCCd}} + \dfrac{3}{2} i_{\mathrm{d}} v_{\mathrm{PCCq}}\right) \end{cases} \quad (11)$$

where K_{p2} and K_{i2} are the proportional gain and integral gain of the power loop.

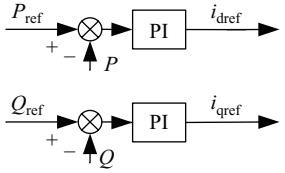

Fig. 8. Outer power loop.

In (11), the decrease of v_{PCCd} from its steady value indicates the power loss in the AC side of the MMC. Thus, the reference value of d-aixs current i_{dref} may show an increasing trend under the grid ground fault, and i_{qref} cannot stay at zero.

When the reference currents vary, the output voltage commands may be changed due to the action of the inner current loop. From the inner current loop shown in Fig. 9, the dq-axis output voltage commands e^*_{vd} and e^*_{vq} can be given by the control equation of the current loop as follows:

$$\begin{cases} e^*_{\mathrm{vd}} = v_{\mathrm{PCCd}} + \omega L_{\mathrm{eq}} i_{\mathrm{q}} + (K_{p1} + K_{i1}\int)(i_{\mathrm{dref}} - i_{\mathrm{d}}) \\ e^*_{\mathrm{vq}} = v_{\mathrm{PCCq}} - \omega L_{\mathrm{eq}} i_{\mathrm{d}} + (K_{p1} + K_{i1}\int)(i_{\mathrm{qref}} - i_{\mathrm{q}}) \end{cases} \tag{12}$$

where K_{p1} and K_{i1} are the proportional gain and the integral gain of the current loop. The amplitude of the equivalent output voltage E_{v}that transfers the influence of the control loop to the PLL can be given as:

$$E_{\mathrm{v}} \approx E^*_{\mathrm{v}} = \sqrt{e^{*2}_{\mathrm{vd}} + e^{*2}_{\mathrm{vq}}} \tag{13}$$

where E^*_{v} is the amplitude of the output voltage commands e^*_{v}. Since the voltage commands in q axis e^*_{vq} varies around zero and the voltage commands in d axis e^*_{vd} is much higher than e^*_{vq}, the variation trend of E^*_{v} is primarily determined by e^*_{vd}.

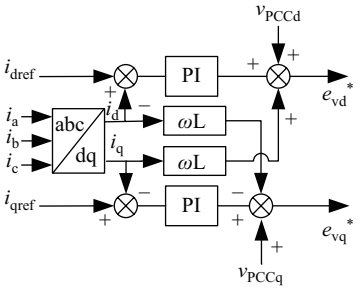

Fig. 9. Inner current loop.

From (12), it can be seen that the variation of the voltage commands e^*_{vd} are primarily affected by v_{PCCd} and i_{dref}. Thus, analyzing whether v_{PCCd} or i_{dref} determine the variation trend of e^*_{vd} is essential. The dominant factor of the variation trend of e^*_{vd} may be related to the control parameters of the inner current loop, such as the proportional gain K_{p1}.

When there is a smaller K_{p1} in the current loop, e^*_{vd} may decline with the decrease of v_{PCCd}. Thus, the amplitude of the output voltage E_{v} may drop to a smaller value according to equation (13). Since φ_1 and φ_2 have opposite signs according to equation (5), we can suppose that the sign of φ_1 is positive as an example. Under this assumption, $\sin\varphi_2$ in Fig. 8 is a negative value, the q-axis voltage at PCC $K_1 V_{\mathrm{g1}} \sin(\varphi_1 + \delta) + K_2 E_{\mathrm{v}} \sin\varphi_2$ may show an increasing tendency. The control loop and the PLL may form a positive feedback. The phase angle difference δ will continue to grow and diverge to infinity, in which case the PLL will become unstable.

When there is a larger K_{p1} in the current loop, e^*_{vd} may become higher with the increase of i_{dref}. The amplitude of the output voltage E_{v} may rise accordingly. With a negative $\sin\varphi_2$ in Fig. 8, $K_1 V_{\mathrm{g1}} \sin(\varphi_1 + \delta) + K_2 E_{\mathrm{v}} \sin\varphi_2$ may decline. The control loop and the PLL may form a negative feedback. The phase angle difference δ will show a convergent tendency and recover to its steady value, in which case the PLL can keep stable.

Similarly, the outer power control loop affects the responses of the PLL by changing the variation trend of e^*_{vd}. When there is a larger proportional gain of the power loop K_{p2}, the system will become more stable. As the d-axis voltage v_{PCCd} decreases because of the phase disturbance, the d-axis reference current i_{dref} will increase. The value of K_{p2} will determine the growth degree of i_{dref} as shown in (11). If there is a larger K_{p2}, i_{dref} will grow more, which causes e^*_{vd} to have an increasing tendency. Then, the control loop and the PLL will form a negative feedback, and the system can recover to a stable state. However, if there is a smaller K_{p2}, the increase of i_{dref} may be slight, and the variation tendency of e^*_{vd} is determined by the drop of v_{PCCd}. Thus, in this situation, the control loop and the PLL may form a positive feedback, and cannot remain stable anymore. The response processes of the PLL with the interaction of the control loop under grid fault are presented in Fig. 10.

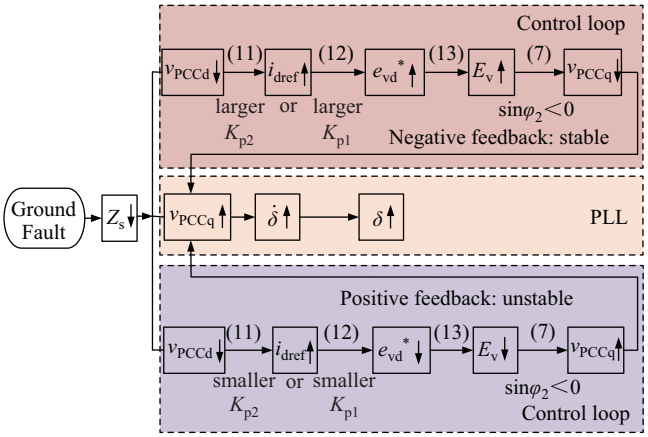

Fig. 10. Response process of PLL with interaction of the control loop under grid fault.

IV. Small-signal Stability Analysis of PLL Considering The Interaction with THE Control Loop

From the qualitative analysis above, how the gains of both the current loop and the power loop affect the stability of the PLL is clarified by the block diagram in Fig. 10. However, to analyze the parameter influence of the system with exact values, a quantitative calculation is needed. In this section, a small-signal model of the PLL considering the interaction of the control loop is established to analyze the small-signal stability and the parameter influence of the PLL after the fault.

According to (6), the linearized small-signal model can be obtained around the steady-state operating point, i.e., $\omega = \omega_{\mathrm{g}}$.

Since the phase angle of the equivalent output voltage θ_{v} is provided by the PLL, θ_{v} is regarded as equal to θ_{PLL} in this paper. Considering the PLL is able to follow the grid phase angle when the system operates in a stable state, the small-

signal equation of (6) can be written as:

$$\begin{cases}\Delta v_{\mathrm{PCCd}} = G_1(\Delta\theta_{\mathrm{g}} - \Delta\theta_{\mathrm{PLL}}) + G_2\Delta\omega + G_3\Delta E_{\mathrm{v}} \\ \Delta v_{\mathrm{PCCq}} = G_4(\Delta\theta_{\mathrm{g}} - \Delta\theta_{\mathrm{PLL}}) + G_5\Delta\omega + G_6\Delta E_{\mathrm{v}}\end{cases} \tag{14}$$

where

$$\begin{cases}G_1 = -K_1(\omega_{\mathrm{g}})V_{\mathrm{g1}}\sin[\varphi_1(\omega_{\mathrm{g}})] \\ G_2 = \{-K_2(\omega_{\mathrm{g}})\sin[\varphi_2(\omega_{\mathrm{g}})]\varphi_2'(\omega_{\mathrm{g}}) \\ \quad + K_2'(\omega_{\mathrm{g}})\cos[\varphi_2(\omega_{\mathrm{g}})]\}E_{\mathrm{v}}(\omega_{\mathrm{g}}) \\ G_3 = K_2(\omega_{\mathrm{g}})\cos[\varphi_2(\omega_{\mathrm{g}})] \\ G_4 = K_1(\omega_{\mathrm{g}})V_{\mathrm{g1}}\cos[\varphi_1(\omega_{\mathrm{g}})] \\ G_5 = \{K_2(\omega_{\mathrm{g}})\cos[\varphi_2(\omega_{\mathrm{g}})]\varphi_2'(\omega_{\mathrm{g}}) \\ \quad + K_2'(\omega_{\mathrm{g}})\sin[\varphi_2(\omega_{\mathrm{g}})]\}E_{\mathrm{v}}(\omega_{\mathrm{g}}) \\ G_6 = K_2(\omega_{\mathrm{g}})\sin[\varphi_2(\omega_{\mathrm{g}})]\end{cases} \tag{15}$$

In (14), ΔE_{v} is the small-signal increment of E_{v}, and $E_{\mathrm{v}}(\omega_{\mathrm{g}})$ is the steady-state value of E_{v} when the angular frequency keeps stable at ω_{g}. In previous studies [18], the output voltage or current of the converter is regarded as the same as the reference values, without considering the dynamic behaviors of the control loop. However, the dynamic of the control loop is taken into consideration in this paper. The calculation of ΔE_{v} will reflect the action of the control loop under the phase disturbance, so it is quite essential to derive the small-signal increment ΔE_{v}.

The small-signal linearized expression of E_{v} can be obtained from (13) when the system operates around the steady-state point ω_{g}, i.e.,

$$\Delta E_{\mathrm{v}} \approx [e_{\mathrm{vd}}^*(\omega_{\mathrm{g}}) + e_{\mathrm{vq}}^*(\omega_{\mathrm{g}})](\Delta e_{\mathrm{vd}}^* + \Delta e_{\mathrm{vq}}^*)/E_{\mathrm{v}}(\omega_{\mathrm{g}}) \tag{16}$$

According to the control equation of the current loop (12), the small-signal items Δe_{vd}^* and Δe_{vq}^* in (16) can be expressed as the linearized inner current control in (17).

$$\begin{cases}\Delta e_{\mathrm{vd}}^* = \Delta v_{\mathrm{PCCd}} + L_{\mathrm{eq}}I_{\mathrm{q}}\Delta\omega + \omega_{\mathrm{g}}L_{\mathrm{eq}}\Delta i_{\mathrm{q}} \\ \qquad + G_i(\Delta i_{\mathrm{dref}} - \Delta i_{\mathrm{d}}) \\ \Delta e_{\mathrm{vq}}^* = \Delta v_{\mathrm{PCCq}} - L_{\mathrm{eq}}I_{\mathrm{d}}\Delta\omega - \omega_{\mathrm{g}}L_{\mathrm{eq}}\Delta i_{\mathrm{d}} \\ \qquad + G_i(\Delta i_{\mathrm{qref}} - \Delta i_{\mathrm{q}})\end{cases} \tag{17}$$

where $G_i = K_{p1} + K_{i1}/\mathrm{s}$.

Similarly, the dq-axis reference current increment Δi_{dref} and Δi_{qref} can be given from the control equation of the power loop (11), i.e.,

$$\begin{cases}\Delta i_{\mathrm{dref}} = \dfrac{3}{2}G_p(-I_{\mathrm{d}}\Delta v_{\mathrm{PCCd}} - V_{\mathrm{PCCd}}\Delta i_{\mathrm{d}} \\ \qquad - I_{\mathrm{q}}\Delta v_{\mathrm{PCC}\ q} - V_{\mathrm{PCCq}}\ \Delta i_{\mathrm{q}}) \\ \Delta i_{\mathrm{qref}} = \dfrac{3}{2}G_p(-I_{\mathrm{q}}\Delta v_{\mathrm{PCCd}} - V_{\mathrm{PCCd}}\Delta i_{\mathrm{q}} \\ \qquad + I_{\mathrm{d}}\Delta v_{\mathrm{PCC}\ q} + V_{\mathrm{PCC}\ q}\Delta i_{\mathrm{d}})\end{cases} \tag{18}$$

where $G_p = K_{p2} + K_{i2}/\mathrm{s}$.

Combining (16), (17) and (18), the small-signal increment of E_{v} can be derived as:

$$\Delta E_{\mathrm{v}} \approx J_1\Delta v_{\mathrm{PCCd}} + J_2\Delta v_{\mathrm{PCCq}} + J_3\Delta i_{\mathrm{d}} + J_4\Delta i_{\mathrm{q}} + J_5\Delta\omega \tag{19}$$

where

$$\begin{cases}J_1 = \left(1 - \dfrac{3}{2}G_iG_pI_{\mathrm{d}} - \dfrac{3}{2}G_iG_pI_{\mathrm{q}}\right)[e_{\mathrm{vd}}^*(\omega_{\mathrm{g}}) \\ \qquad + e_{\mathrm{vq}}^*(\omega_{\mathrm{g}})]/E_{\mathrm{v}}(\omega_{\mathrm{g}}) \\ J_2 = \left(1 + \dfrac{3}{2}G_iG_pI_{\mathrm{d}} - \dfrac{3}{2}G_iG_pI_{\mathrm{q}}\right)[e_{\mathrm{vd}}^*(\omega_{\mathrm{g}}) \\ \qquad + e_{\mathrm{vq}}^*(\omega_{\mathrm{g}})]/E_{\mathrm{v}}(\omega_{\mathrm{g}}) \\ J_3 = \left(\dfrac{3}{2}G_iG_pV_{\mathrm{PCCq}} - \dfrac{3}{2}G_iG_pV_{\mathrm{PCCd}} - G_i - \omega_{\mathrm{g}}L_{\mathrm{eq}}\right) \\ \qquad [e_{\mathrm{vd}}^*(\omega_{\mathrm{g}}) + e_{\mathrm{vq}}^*(\omega_{\mathrm{g}})]/E_{\mathrm{v}}(\omega_{\mathrm{g}}) \\ J_4 = \left(\omega_{\mathrm{g}}L_{\mathrm{eq}} - \dfrac{3}{2}G_iG_pV_{\mathrm{PCCq}} - \dfrac{3}{2}G_iG_pV_{\mathrm{PCCd}} - G_i\right) \\ \qquad [e_{\mathrm{vd}}^*(\omega_{\mathrm{g}}) + e_{\mathrm{vq}}^*(\omega_{\mathrm{g}})]/E_{\mathrm{v}}(\omega_{\mathrm{g}}) \\ J_5 = L_{\mathrm{eq}}(I_{\mathrm{q}} - I_{\mathrm{d}})[e_{\mathrm{vd}}^*(\omega_{\mathrm{g}}) + e_{\mathrm{vq}}^*(\omega_{\mathrm{g}})]/E_{\mathrm{v}}(\omega_{\mathrm{g}})\end{cases} \tag{20}$$

Considering the relationship of the grid voltage and current in Fig. 5, the grid voltage and current should satisfy the following equation:

$$\begin{aligned}I_{\mathrm{g}}\angle\theta_i &= \frac{1}{Z_{\mathrm{s}}(\omega_{\mathrm{PLL}}) + Z_{\mathrm{eq}}(\omega_{\mathrm{PLL}})}E_{\mathrm{v}}\angle\theta_{\mathrm{v}} \\ &\quad - \frac{1}{Z_{\mathrm{s}}(\omega_{\mathrm{g}}) + Z_{\mathrm{eq}}(\omega_{\mathrm{g}})}V_{\mathrm{g1}}\angle\theta_{\mathrm{g}} \\ &= K_3(\omega_{\mathrm{PLL}})E_{\mathrm{v}}e^{j[\theta_{\mathrm{v}} + \varphi_3(\omega_{\mathrm{PLL}})]} \\ &\quad - K_3(\omega_{\mathrm{g}})V_{\mathrm{g1}}e^{j[\theta_{\mathrm{g}} + \varphi_3(\omega_{\mathrm{g}})]}\end{aligned} \tag{21}$$

where

$$K_3(\omega) = \frac{1}{|Z_{\mathrm{s}}(\omega) + Z_{\mathrm{eq}}(\omega)|},$$
$$\varphi_3(\omega) = \mathrm{phase}\left(\frac{1}{Z_{\mathrm{s}}(\omega) + Z_{\mathrm{eq}}(\omega)}\right)$$

Thus, Δi_{d} and Δi_{q} in (19) can be given as:

$$\begin{cases}\Delta i_{\mathrm{d}} = H_1\Delta\omega + H_2\Delta e_{vm} + H_3(\Delta\theta_{\mathrm{g}} - \Delta\theta_{\mathrm{PLL}}) \\ \Delta i_{\mathrm{q}} = H_4\Delta\omega + H_5\Delta e_{vm} + H_6(\Delta\theta_{\mathrm{g}} - \Delta\theta_{\mathrm{PLL}})\end{cases} \tag{22}$$

where

$$\begin{cases}H_1 = K_3'(\omega_{\mathrm{g}})E_{\mathrm{v}}(\omega_{\mathrm{g}})\cos[\varphi_3(\omega_{\mathrm{g}})] \\ \qquad - K_3E_{\mathrm{v}}(\omega_{\mathrm{g}})\varphi_3'(\omega_{\mathrm{g}})\sin[\varphi_3(\omega_{\mathrm{g}})] \\ H_2 = K_3(\omega_{\mathrm{g}})\cos[\varphi_3(\omega_{\mathrm{g}})] \\ H_3 = K_3(\omega_{\mathrm{g}})V_{\mathrm{g1}}\sin[\varphi_3(\omega_{\mathrm{g}})] \\ H_4 = K_3'(\omega_{\mathrm{g}})E_{\mathrm{v}}(\omega_{\mathrm{g}})\sin[\varphi_3(\omega_{\mathrm{g}})] \\ \qquad + K_3(\omega_{\mathrm{g}})E_{\mathrm{v}}(\omega_{\mathrm{g}})\varphi_3'(\omega_{\mathrm{g}})\cos[\varphi_3(\omega_{\mathrm{g}})] \\ H_5 = K_3(\omega_{\mathrm{g}})\sin[\varphi_3(\omega_{\mathrm{g}})] \\ H_6 = -K_3(\omega_{\mathrm{g}})V_{\mathrm{g1}}\cos[\varphi_3(\omega_{\mathrm{g}})]\end{cases} \tag{23}$$

Combining (22) and (19), there is:

$$\begin{aligned}\Delta E_{\mathrm{v}} &= \frac{J_3H_1 + J_4H_4 + J_5}{1 - J_3H_2 - J_4H_5}\Delta\omega + \frac{J_1}{1 - J_3H_2 - J_4H_5}\Delta v_{\mathrm{PCCd}} \\ &\quad + \frac{J_2}{1 - J_3H_2 - J_4H_5}\Delta v_{\mathrm{PCCq}} \\ &\quad + \frac{J_3H_3 + J_4H_6}{1 - J_3H_2 - J_4H_5}(\Delta\theta_{\mathrm{g}} - \Delta\theta_{\mathrm{PLL}}) \\ &= T_1\Delta\omega + T_2\Delta v_{\mathrm{PCCd}} + T_3\Delta v_{\mathrm{PCCq}} + T_4(\Delta\theta_{\mathrm{g}} - \Delta\theta_{\mathrm{PLL}})\end{aligned} \tag{24}$$

And then substituting (24) into (14), Δv_{PCCq} can be rewritten with only three small-signal items that are related to frequency and angle, i.e., $\Delta\omega$, $\Delta\theta_{\mathrm{g}}$ and $\Delta\theta_{\mathrm{PLL}}$, as shown in (25).

$$\Delta v_{\mathrm{PCCq}} = F_1\Delta\omega + F_2(\Delta\theta_{\mathrm{g}} - \Delta\theta_{\mathrm{PLL}}) \tag{25}$$

where

$$\begin{cases} F_1 = \dfrac{(G_5+G_6T_1)(1-G_3T_2)+G_6T_2(G_2+G_3T_1)}{(1-G_3T_2)(1-G_6T_3)-G_6T_2G_3T_3} \\ F_2 = \dfrac{(G_4+G_6T_4)(1-G_3T_2)+G_6T_2(G_1+G_3T_4)}{(1-G_3T_2)(1-G_6T_3)-G_6T_2G_3T_3} \end{cases} \tag{26}$$

Then, the small-signal model of the PLL in the grid-connected MMC system can be established in (27) and the model around the operating point can be also described in Fig. 11. The red part of Fig. 11 shows the influence of the control loop on the PLL. In Fig. 11, the interaction between the PLL and the control loop is presented clearly. The control loop affects the PLL by changing the output voltage of the MMC ΔE_{v}, and the output phase $\Delta\theta_{\mathrm{PLL}}$ and angular frequency $\Delta\omega$ of the PLL will further affect the output voltage of the control loop ΔE_{v}.

$$\Delta\theta_{\mathrm{PLL}} = [F_1\Delta\omega + F_2(\Delta\theta_{\mathrm{g}} - \Delta\theta_{\mathrm{PLL}})]\left(K_p + \frac{K_i}{s}\right)\frac{1}{s} \tag{27}$$

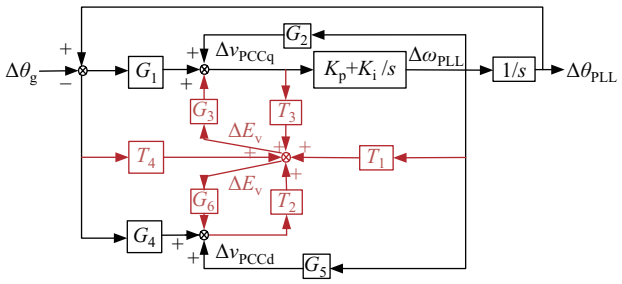

Fig. 11. Small-signal model of PLL.

According to (27), the input and output transfer function of the PLL can be derived as follows:

$$\frac{\Delta\theta_{\mathrm{PLL}}}{\Delta\theta_{\mathrm{g}}} = \frac{K_pF_2s+K_iF_2}{(1-K_pF_1)s^2+(K_pF_2-K_iF_1)s+K_iF_2} = \frac{N(s)}{D(s)} \tag{28}$$

Solving the poles of the transfer function (28), the stability of the PLL can be assessed by analyzing the sign of the real parts of the poles. When there is no pole in the right half-plane, the PLL can remain stable after the fault. On the contrary, if there is any pole staying in the right half-plane, the PLL will lose stability.

V. Verification

In this section, a grid-connected three-phase 21-level MMC simulation model is built in the PSCAD platform to verify the analysis of the response process in Fig. 10. The simulation model is shown in Fig. 1 and Fig. 2, and the parameters of the grid-connected MMC system are listed in Table I.

TABLE I
Parameters of Grid-connected MMC system

System parameter	Value
AC voltage v_{g} (kV)	23
Phase of AC voltage θ_{g} (deg)	0
Rated DC voltage V_{dc} (kV)	40
Number of SMs per arm N	20
SM capacitance C (mF)	10
Reference value of active power P_{ref} (MW)	40
Reference value of reactive power Q_{ref} (MVar)	0
Proportional gain of PLL K_p	0.2
Integral gain of PLL K_i	100
AC grid frequency f_{g} (Hz)	50
Arm impedance $Z_0(L_0, R_0)$ (mH, Ω)	16, 0.18
AC filter impedance $Z_{\mathrm{f}}(L_{\mathrm{f}}, R_{\mathrm{f}})$ (mH, Ω)	0.1, 0.1
Series impedance $Z_{\mathrm{g}}(L_{\mathrm{g}}, R_{\mathrm{g}})$ (mH, Ω)	0.1, 0.2
Impedance of line 1 $Z_{\mathrm{line1}}(L_{\mathrm{line1}}, R_{\mathrm{line1}})$ (mH, Ω)	13, 0.2
Impedance of line 2 $Z_{\mathrm{line2}}(L_{\mathrm{line2}}, R_{\mathrm{line2}})$ (mH, Ω)	29, 0.2
Ground impedance $Z_{\mathrm{gnd}}(L_{\mathrm{gnd}}, R_{\mathrm{gnd}})$ (mH, Ω)	25, 0.1

In the MMC system, when a ground fault occurs in line 2, the grid impedance Z_{s} changes from $Z_{\mathrm{g}} + (Z_{\mathrm{line1}}//Z_{\mathrm{line2}})$ to $(Z_{\mathrm{g}} + (Z_{\mathrm{line1}}//Z_{\mathrm{line2}}))//Z_{\mathrm{gnd}}$. The equivalent grid voltage changes from v_{g} to v_{g1}. The amplitude and the phase of the voltage at PCC may change accordingly, and then induce some dynamic behaviors of the PLL. To analyze the transient responses of the PLL influenced by the control loop under the ground fault, simulations with different control parameters are presented in this section.

A. Parameter Influence of K_{p1}

Figure 12 and Fig. 13 show the transient responses of the grid-connected MMC when the ground fault happens at 6 s with different proportional gains of the current loop K_{p1}.

When $K_{p1} = 10$, $K_{i1} = 0.5$, the system presents an abnormal operating state, as shown in Fig. 12. A divergent oscillation can be observed in the output angular frequency of the PLL. The active power shows a slight decrease and then recovers to its steady value. The reactive power, dq-axis voltage and current also oscillate and diverge with the divergency of the PLL output angular frequency. The AC voltage at PCC and AC grid current shows distortion due to the oscillations in the dq-axis voltage and current after the ground fault, which can be shown by the waveforms $v_{\mathrm{PCC}a}$ and $i_{\mathrm{g}a}$ in Fig. 12 (e)–(f). The waveforms in Fig. 12 verify the analysis that the PLL may lose stability after the fault with a smaller K_{p1}.

When $K_{p1} = 45$, $K_{i1} = 0.5$, the system presents a tendency to recover to a stable state, as shown in Fig. 13. From Fig. 13 (a), it can be seen that the output angular frequency of the PLL starts to oscillate after the fault, but the amplitude of the oscillation is within ± 20 rad/s and shows a convergent trend. In Fig. 13 (b), the active power drops slightly and then recovers to its steady state, and the reactive power shows a slight oscillation. Fig. 13 (c) and (d) present the dq-axis voltage and current. The d-axis voltage at PCC decreases to 12.7 kV because of the grid fault, while the d-axis current increases to 2 kA. The q-axis voltage and current still stay at zero accompanied with slight convergent oscillations, which almost have no influence on the AC voltage at PCC $v_{\mathrm{PCC}a}$ and AC grid current waveforms $i_{\mathrm{g}a}$, as shown in Fig. 13 (e)–

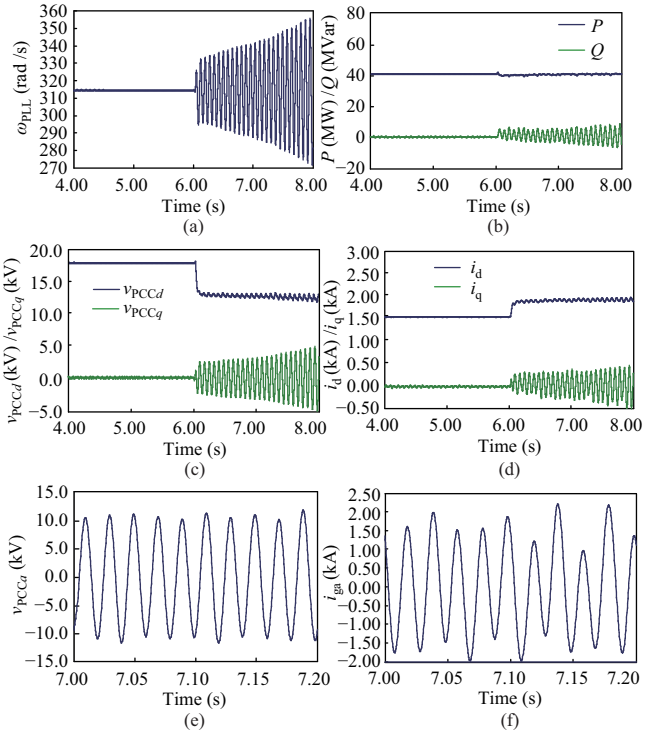

Fig. 12. Unstable transient responses of MMC when $K_{p1} = 10$. (a) Output angular frequency of PLL. (b) Active power/reactive power. (c) dq-axis voltage at PCC. (d) dq-axis grid current. (e) PCC voltage in phase a. (f) Grid current in phase a.

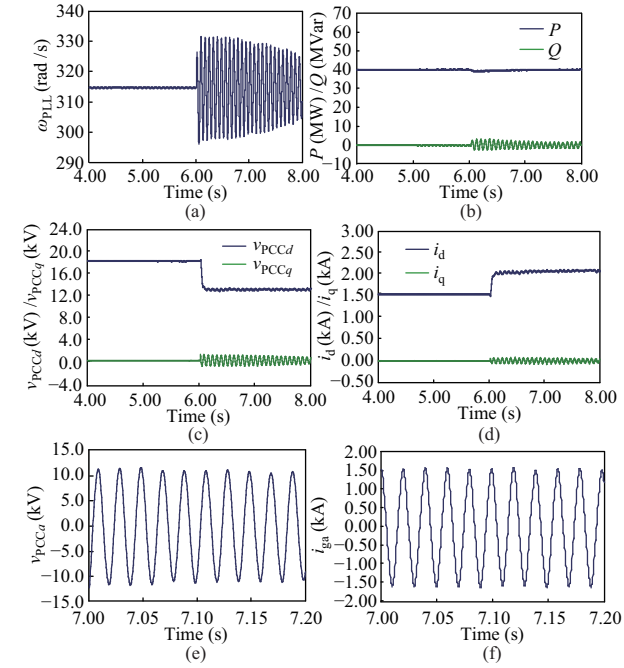

Fig. 13. Stable transient responses of MMC when $K_{p1} = 45$. (a) Output angular frequency of PLL. (b) Active power/reactive power. (c) dq-axis voltage at PCC. (d) dq-axis grid current. (e) PCC voltage in phase a. (f) Grid current in phase a.

(f). The waveforms in Fig. 13 verify the analysis that the PLL is able to remain stable after the fault when there is a larger K_{p1}.

Comparing the above two responses, the stability of the PLL under the grid fault is changed due to the variation of the current loop proportional gain. From the simulation results, it can be shown that a larger proportional gain of the inner current loop may improve the stability of the PLL in a grid-connected MMC system under grid faults.

B. Parameter Influence of K_{p2}

Figure 14 shows the waveform of the MMC system when the proportional gain of the outer power loop K_{p2} is set as 5, and other parameters are the same as the parameters in Fig. 12, where $K_{p2} = 0.5$. Thus, the comparison of Fig. 14 and Fig. 12 can show the parameter influence of the outer power loop. As shown in Fig. 14, there are convergent oscillations in the waveforms of the output angular frequency of the PLL, the reactive power, the q-axis voltage and the q-axis current. Thus, it can be shown that the PLL has a tendency of recovering to a stable state with a larger K_{p2}.

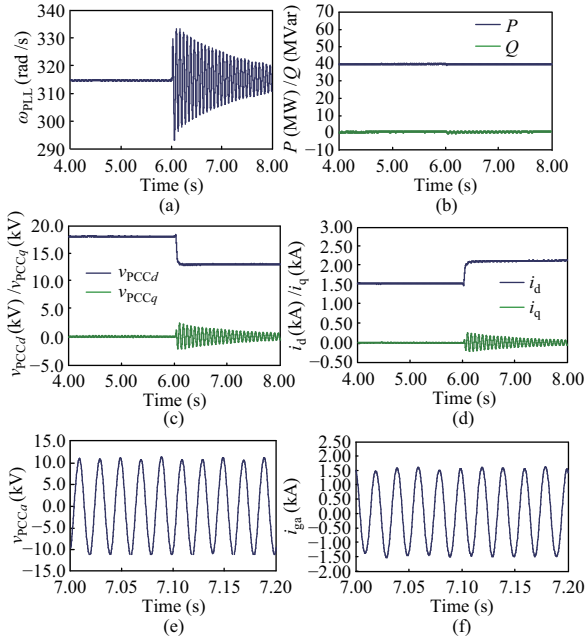

Fig. 14. Stable transient responses of MMC when $K_{p2} = 5$. (a) Output angular frequency of PLL. (b) Active power/reactive power. (c) dq-axis voltage at PCC. (d) dq-axis grid current. (e) PCC voltage in phase a. (f) Grid current in phase a.

C. Parameter Influence of K_p

As the proportional gain of the PLL K_p is a quite essential parameter that has a great impact on the stability of the PLL, the influence of parameter K_p is also analyzed in this section.

When the proportional gain K_p decreases to 0.18 and the integral gain K_i remains unchanged at 100, the response waveforms of the grid-connected MMC under the ground fault with different current loop gains K_{p1} are presented in Fig. 15 and Fig. 16.

Figure 15 shows the transient responses of the MMC with the same current loop parameters as Fig. 13, i.e., $K_{p1} = 45$, $K_{i1} = 0.5$. With a smaller proportional gain K_p, the PLL cannot remain stable. The waveforms of the PLL output angular frequency, the reactive power, the q-axis voltage component

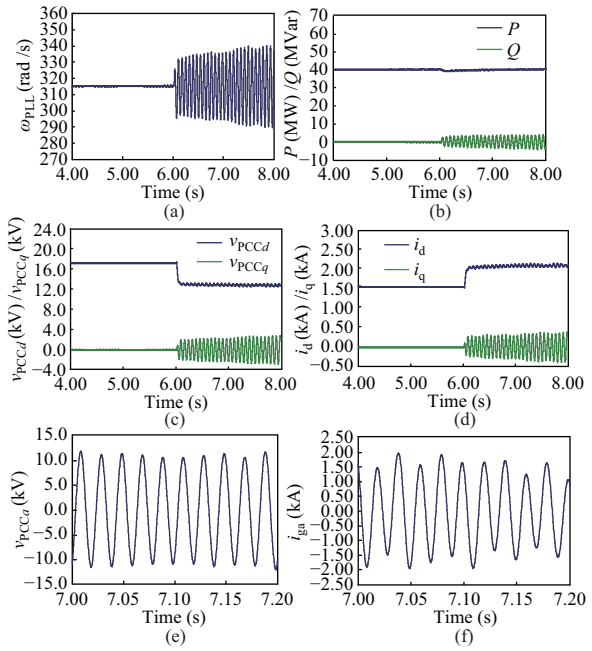

Fig. 15. Unstable transient responses of MMC when $K_{p1} = 45$. (a) Output angular frequency of PLL. (b) Active power/reactive power. (c) dq-axis voltage at PCC. (d) dq-axis grid current. (e) PCC voltage in phase a. (f) Grid current in phase a.

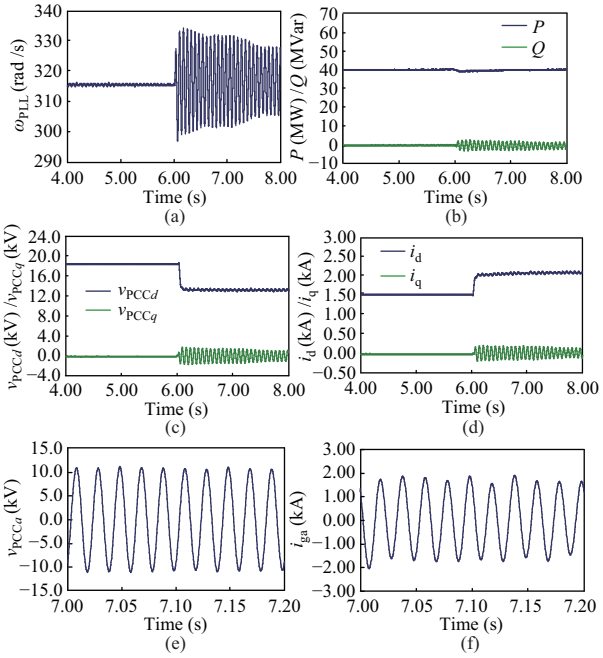

Fig. 16. Stable transient responses of MMC when $K_{p1} = 55$. (a) Output angular frequency of PLL. (b) Active power/reactive power. (c) dq-axis voltage at PCC. (d) dq-axis grid current. (e) PCC voltage in phase a. (f) Grid current in phase a.

and the q-axis current component present divergent tendencies when the ground fault occurs, as shown in Fig. 15 (a)–(d). Due to the divergent oscillations, there will be waveform distortion in the PCC voltage and the grid current, as shown in Fig. 15 (e)–(f).

According to the parameter analysis of the current loop proportional gain K_{p1}, it can be shown that the increase of the current loop gain K_{p1} is able to improve the stability of the PLL. In Fig. 16, a larger current loop gain K_{p1} is set in the MMC system, where $K_{p1} = 55$ and $K_{i1} = 0.5$. Under this parameter condition, convergent oscillations can be seen in the PLL output angular frequency, the reactive power, the q-axis voltage and current components, which means that the MMC system is able to recover to a steady state and these oscillations will disappear after a finite time.

From the transient responses under a decreased proportional gain K_p, it can be concluded that a smaller K_p may have an adverse influence on the stability of the PLL. In addition, the critical value of K_{p1} in this MMC system will become larger when the proportional gain K_p declines. Thus, with a smaller PLL gain K_p, a larger current loop gain K_{p1} is needed to improve the stability of the PLL.

D. Verification of Small-signal Stability Analysis

Figure 17 present the pole-zero analysis results of the transfer function (24) when the system operates within the parameters in Fig. 12 and Fig. 13. When $K_{p1} = 10$, the pole-zero map can be seen in Fig. 17 (a). There is a pair of poles p_3 and p_4 in the right half plane, which means that PLL loses its stability. The stability analysis results and the simulation results shown in Fig. 12 match well. When $K_{p1} = 45$, all the poles are at the left half plane, confirming that the PLL can remain stable under such parameters. The pole-zero mapping of the transfer function is also in agreement with the simulation results shown in Fig. 13.

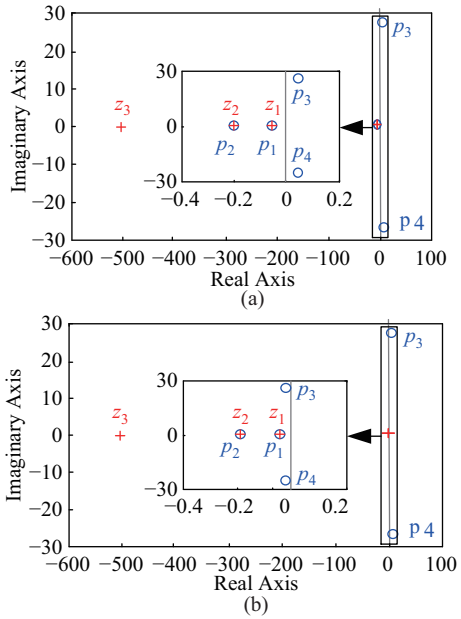

Fig. 17. Simulation results and pole-zero maps of the PLL under phase disturbance. (a) Pole-zero map of the small-signal model when $K_{p1} = 10$. (b) Pole-zero map of the small-signal model when $K_{p1} = 45$.

From Fig. 17, the effectiveness of the small-signal model and the stability analysis method presented in Section IV is verified, which also illustrates that the small-signal stability of the PLL can be affected by the parameter of the control loop. With the increase of the proportional gain K_{p1}, a pair of poles may cross the imaginary axis to the right half plane. Thus, the

PLL can be more stable with a higher proportional gain of the current control loop. The stability analysis of the small-signal model can be used in the parameter design of grid-connected systems.

E. Experimental Verification

To further verify the analysis of the control loop's parameter influence on the PLL, down-scale hardware-in-the-loop (HIL) experiments with a two-level voltage-source inverter are performed in this section. The topology of the three-phase voltage-source inverter is shown in Fig. 18. And the circuit parameters are listed in Table II. The circuit of the three-phase voltage-source inverter is established in the RT-LAB platform and the control part is achieved by a practical controller (STM32F401) with a FPGA (EP4CE115F23C7).

TABLE II
PARAMETERS OF TWO-LEVEL VOLTAGE-SOURCE INVERTER

Parameter	Value	Parameter	Value
$V_{\rm dc}$	40 kV	$Z_{\rm g}$	0.1 mH, 0.2 Ω
$R_{\rm dc}$	0.01 Ω	$Z_{\rm ac}$	2 mH, 1 Ω
C	16 mF	$Z_{\rm line1}$	13 mH, 0.2 Ω
$v_{\rm g}$	23 kV	$Z_{\rm line2}$	18 mH, 2 Ω
K_p/K_i	0.01/2	$Z_{\rm gnd}$	29 mH, 0.1 Ω

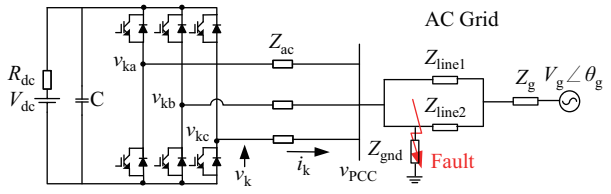

Fig. 18. Topology of the three-phase voltage-source inverter.

The HIL experimental results of PLL's output angular frequency with different control parameters are presented in Fig. 19. The output angular frequency of the PLL diverges as soon as grid fault occurs when $K_{p1} = 1.8$, as shown in Fig. 19 (a). However, when there is a larger K_{p1}, i.e., $K_{p1} = 2.4$, the output angular frequency recovers to the steady-state operating point ($\omega_{\rm PLL} = \omega_{\rm g} = 314$ rad/s) as shown in Fig. 19 (b). From the experimental results, the theory analysis of the PLL influenced by the dynamics of the control loop can be further validated.

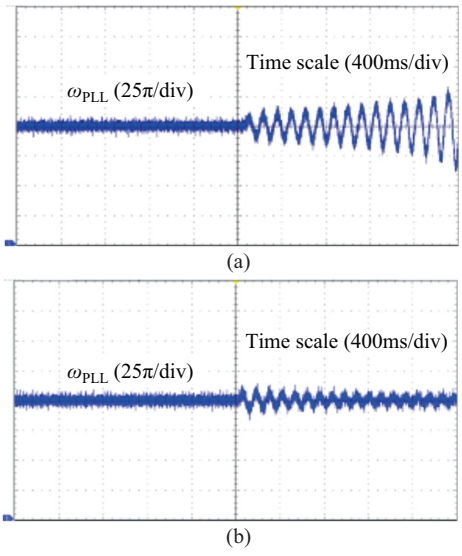

Fig. 19. Experimental results of PLL's output angular frequency with different control loop parameters. (a) Unstable response when $K_{p1} = 1.8$. (b) Stable response when $K_{p1} = 2.4$.

VI. CONCLUSION

In the practical grid-connected power electronics converter system, the responses of PLL are not only determined by their own parameters, but are also related to the control loops. In this study, the post fault response process of the PLL considering the influence of the control loop is investigated in a grid-connected MMC system. By establishing the equivalent model of the PLL with the interaction of the control loop, the influence of the control loop on the behaviors of the PLL can be analyzed. A small-signal model and the corresponding pole-zero map are proposed to provide a qualitative stability assessment. It is shown that when the control loops have a lower proportional gain and form a positive feedback with the PLL under a certain parameter condition, the system will lose stability. It can be concluded that the stability of the PLL can be influenced by the dynamics of the control loop, and destabilized by the grid-connected system during a transient fault.

REFERENCES

[1] L. B. Huang, H. H. Xin, and Z. Wang, "Damping low-frequency oscillations through VSC-HVDC stations operated as virtual synchronous machines," *IEEE Transactions on Power Electronics*, vol. 34, no. 6, pp. 5803–5818, Jun. 2019.

[2] W. J. Du, Q. Fu, and H. F. Wang, "Power system small-signal angular stability affected by virtual synchronous generators," *IEEE Transactions on Power Systems*, vol. 34, no. 4, pp. 3209–3219, Jul. 2019.

[3] E. Ebrahimzadeh, F. Blaabjerg, X. F. Wang, and C. L. Bak, "Optimum design of power converter current controllers in large-scale power electronics based power systems," *IEEE Transactions on Industry Applications*, vol. 55, no. 3, pp. 2792–2799, May/Jun. 2019.

[4] W. Dong, H. H. Xin, D. Wu, and L. B. Huang, "Small signal stability analysis of multi-infeed power electronic systems based on grid strength assessment," *IEEE Transactions on Power Systems*, vol. 34, no. 2, pp. 1393–1403, Mar. 2019.

[5] X. F. Wang and F. Blaabjerg, "Harmonic stability in power electronic-based power systems: concept, modeling, and analysis," *IEEE Transactions on Smart Grid*, vol. 10, no. 3, pp. 2858–2870, May 2019.

[6] A. Bidadfar, H. P. Nee, L. D. Zhang, L. Harnefors, S. Namayantavana, M. Abedi, M. Karrari, and G. B. Gharehpetian, "Power system stability analysis using feedback control system modeling including hvdc transmission links," *IEEE Transactions on Power Systems*, vol. 31, no. 1, pp. 116–124, Jan. 2016.

[7] B. Wen, D. Dong, D. Boroyevich, R. Burgos, P. Mattavelli, and Z. Y. Shen, "Impedance-based analysis of grid-synchronization stability for three-phase paralleled converters," *IEEE Transactions on Power Electronics*, vol. 31, no. 1, pp. 26–38, Jan. 2016.

[8] Y. F. Wen, J. P. Zhan, C. Y. Chung, and W. Y. Li, "Frequency stability enhancement of integrated AC/VSC-MTDC systems with massive infeed of offshore wind generation," *IEEE Transactions on Power Systems*, vol. 33, no. 5, pp. 5135–5146, Sep. 2018.

[9] F. Nejabatkhah, Y. W. Li, K. Sun, and R. X. Zhang, "Active power oscillation cancelation with peak current sharing in parallel interfacing converters under unbalanced voltage," *IEEE Transactions on Power Electronics*, vol. 33, no. 12, pp. 10200–10214, Dec. 2018.

[10] A. A. A. Radwan and Y. A. R. I. Mohamed, "Improved vector control strategy for current-source converters connected to very weak grids," *IEEE Transactions on Power Systems*, vol. 31, no. 4, pp. 3238–3248, Jul. 2016.

[11] I. Carugati, P. Donato, S. Maestri, D. Carrica, and M. Benedetti, "Frequency adaptive PLL for polluted single-phase grids," *IEEE Transactions on Power Electronics*, vol. 27, no. 5, pp. 2396–2404, May 2012.
[12] M. G. Taul, X. F. Wang, P. Davari, and F. Blaabjerg, "An overview of assessment methods for synchronization stability of grid-connected converters under severe symmetrical grid faults," *IEEE Transactions on Power Electronics*, vol. 34, no. 10, pp. 9655–9670, Oct. 2019.
[13] M. Huang, Y. Peng, C. K. Tse, Y. S. Liu, J. J. Sun, and X. M. Zha, "Bifurcation and large-signal stability analysis of three-phase voltage source converter under grid voltage dips," *IEEE Transactions on Power Electronics*, vol. 32, no. 11, pp. 8868–8879, Nov. 2017.
[14] S. Mortazavian, M. M. Shabestary, and Y. A. R. I. Mohamed, "Analysis and dynamic performance improvement of grid-connected voltage–source converters under unbalanced network conditions," *IEEE Transactions on Power Electronics*, vol. 32, no. 10, pp. 8134–8149, Oct. 2017.
[15] Q. Hu, L. J. Fu, F. Ma, and F. Ji, "Large signal synchronizing instability of PLL-based VSC connected to weak AC grid," *IEEE Transactions on Power Systems*, vol. 34, no. 4, pp. 3220–3229, Jul. 2019.
[16] M. G. Taul, X. F. Wang, P. Davari, and F. Blaabjerg, "Robust fault ridethrough of converter-based generation during severe faults with phase jumps," *IEEE Transactions on Industry Applications*, vol. 56, no. 1, pp. 570–583, Jan. /Feb. 2020.
[17] Y. Z. Chang, J. B. Hu, W. Q. Y. Tang, and G. B. Song, "Fault current analysis of Type-3 WTs considering sequential switching of internal control and protection circuits in multi time scales during LVRT," *IEEE Transactions on Power Systems*, vol. 33, no. 6, pp. 6894–6903, Nov. 2018.
[18] D. Dong, B. Wen, P. Mattavelli, D. Boroyevich, and Y. S. Xue, "Grid-synchronization modeling and its stability analysis for multi-paralleled three-phase inverter systems," in *2013 Twenty-Eighth Annual IEEE Applied Power Electronics Conference and Exposition*, Long Beach, CA, 2013, pp. 439–446.
[19] H. Wu and X. F. Wang, "Transient stability impact of the phase-locked loop on grid-connected voltage source converters," in *2018 International Power Electronics Conference*, Niigata, 2018, pp. 2673–2680.
[20] X. F. Wang, L. Harnefors, and F. Blaabjerg, "Unified impedance model of grid-connected voltage-source converters," *IEEE Transactions on Power Electronics*, vol. 33, no. 2, pp. 1775–1787, Feb. 2018.
[21] D. Dong, B. Wen, D. Boroyevich, P. Mattavelli, and Y. S. Xue, "Analysis of phase-locked loop low-frequency stability in three-phase grid-connected power converters considering impedance interactions," *IEEE Transactions on Industrial Electronics*, vol. 62, no. 1, pp. 310–321, Jan. 2015.
[22] H. Wu and X. F. Wang, "Design-oriented transient stability analysis of grid-connected converters with power synchronization control," *IEEE Transactions on Industrial Electronics*, vol. 66, no. 8, pp. 6473–6482, Aug. 2019.
[23] H. Wu and X. F. Wang, "Transient angle stability analysis of grid-connected converters with the first-order active power loop," in *2018 IEEE Applied Power Electronics Conference and Exposition*, San Antonio, TX, 2018, pp. 3011–3016.
[24] L. B. Huang, H. H. Xin, Z. Wang, L. Q. Zhang, K. Y. Wu, and J. B. Hu, "Transient stability analysis and control design of droop-controlled voltage source converters considering current limitation," *IEEE Transactions on Smart Grid*, vol. 10, no. 1, pp. 578–591, Jan. 2019.
[25] L. Harnefors, L. Zhang, and M. Bongiorno, "Frequency-domain passivity-based current controller design," *IET Power Electronics*, vol. 1, no. 4, pp. 455–465, Dec. 2008.

Yushuang Liu (S'18) received her B.Eng. degree in Electrical Engineering in 2016 from Wuhan University, Wuhan, China, where she is currently working toward her Ph.D. degree. Since October 2019, she has been a visiting Ph.D. student with the Department of Electrical, Electronic and Computer Engineering, at the University of Western Australia, Australia. Her main research interests include the modeling and stability analysis of power converters.

Meng Huang (S'11–M'13) received his B.Eng. and M.Eng. degrees in Electronic Science and Technology from the Huazhong University of Science and Technology, Wuhan, China, in 2006 and 2008, respectively, and his Ph.D. degree in Power Electronics from Hong Kong Polytechnic University, Hong Kong, China, in 2013. He is currently an Associate Professor with the School of Electrical Engineering and Automation, Wuhan University, Wuhan, China. His research interests include nonlinear analysis of power converters and power electronics reliability.

Xiaoming Zha (M'02) received his B.S., M.S., and Ph.D. degrees in Electrical Engineering from Wuhan University, Wuhan, China, in 1989, 1992, and 2001, respectively. He was a Postdoctoral Fellow with the University of Alberta, Canada, from 2001 to 2003. He has been a Faculty Member of Wuhan University since 1992, and became a Professor in 2003. He is currently the Deputy Dean with the School of Electrical Engineering and Automation, Wuhan University. His research interests include power electronic converters, the application of power electronics in smart grids and renewable energy generation, the analysis and control of microgrids, the analysis and control of power quality, and frequency control of high-voltage high-power electric motors.

Herbert Ho-Ching Iu (S'98–M'00–SM'06) received the B.Eng. (Hons.) degree in Electrical and Electronic Engineering from the University of Hong Kong, Hong Kong, China, in 1997. He received the Ph.D. degree in Electronic and Information Engineering from the Hong Kong Polytechnic University, Hong Kong, China, in 2000. In 2002, he joined the School of Electrical, Electronic and Computer Engineering, The University of Western Australia, Perth, WA, Australia, where he is currently a Professor. His research interests include power electronics, renewable energy, nonlinear dynamics, current sensing techniques, and memristive systems. Prof. Iu currently serves as an Associate Editor of IEEE Transactions on Power Electronics, IEEE Transactions on Smart Grids, IEEE Transactions on Network Science and Engineering, IEEE Transactions on Circuits and Systems-II, and IEEE Access.